



TECH BRIEFS

NATIONAL AERONAUTICS AND SPACE ADMINISTRATION

-  **Technology Focus**
-  **Electronics/Computers**
-  **Software**
-  **Materials**
-  **Mechanics/Machinery**
-  **Manufacturing**
-  **Bio-Medical**
-  **Physical Sciences**
-  **Information Sciences**
-  **Books and Reports**

INTRODUCTION

Tech Briefs are short announcements of innovations originating from research and development activities of the National Aeronautics and Space Administration. They emphasize information considered likely to be transferable across industrial, regional, or disciplinary lines and are issued to encourage commercial application.

Additional Information on NASA Tech Briefs and TSPs

Additional information announced herein may be obtained from the NASA Technical Reports Server: <http://ntrs.nasa.gov>.

Please reference the control numbers appearing at the end of each Tech Brief. Information on NASA's Innovative Partnerships Program (IPP), its documents, and services is available on the World Wide Web at <http://www.ipp.nasa.gov>.

Innovative Partnerships Offices are located at NASA field centers to provide technology-transfer access to industrial users. Inquiries can be made by contacting NASA field centers listed below.

NASA Field Centers and Program Offices

Ames Research Center

David Morse
(650) 604-4724
david.r.morse@nasa.gov

Dryden Flight Research Center

Ron Young
(661) 276-3741
ronald.m.young@nasa.gov

Glenn Research Center

Kimberly A. Dalgleish-Miller
(216) 433-8047
kimberly.a.dalgleish@nasa.gov

Goddard Space Flight Center

Nona Cheeks
(301) 286-5810
nona.k.cheeks@nasa.gov

Jet Propulsion Laboratory

Indrani Graczyk
(818) 354-2241
indrani.graczyk@jpl.nasa.gov

Johnson Space Center

John E. James
(281) 483-3809
john.e.james@nasa.gov

Kennedy Space Center

David R. Makufka
(321) 867-6227
david.r.makufka@nasa.gov

Langley Research Center

Michelle Ferebee
(757) 864-5617
michelle.t.ferebee@nasa.gov

Marshall Space Flight Center

Terry L. Taylor
(256) 544-5916
terry.taylor@nasa.gov

Stennis Space Center

Ramona Travis
(228) 688-3832
ramona.e.travis@ssc.nasa.gov

NASA Headquarters

Daniel Lockney,
Technology Transfer Program Executive
(202) 358-2037
daniel.p.lockney@nasa.gov

Small Business Innovation Research (SBIR) & Small Business Technology Transfer (STTR) Programs

Rich Leshner, Program Executive
(202) 358-4920
rleshner@nasa.gov



TECH BRIEFS

NATIONAL AERONAUTICS AND SPACE ADMINISTRATION



5 Technology Focus: Sensors

- 5 Instrument Suite for Vertical Characterization of the Ionosphere-Thermosphere System
- 5 Terahertz Radiation Heterodyne Detector Using Two-Dimensional Electron Gas in a GaN Heterostructure
- 6 Pattern Recognition Algorithm for High-Sensitivity Odorant Detection in Unknown Environments
- 6 Determining Performance Acceptability of Electrochemical Oxygen Sensors
- 7 Versatile Controller for Infrared Lamp and Heater Arrays
- 7 High-Speed Scanning Interferometer Using CMOS Image Sensor and FPGA Based on Multifrequency Phase-Tracking Detection
- 7 Ultra-Low-Power MEMS Selective Gas Sensors



9 Electronics/Computers

- 9 Compact Receiver Front Ends for Submillimeter-Wave Applications
- 9 Dynamically Reconfigurable Systolic Array Accelerator
- 9 Blocking Losses With a Photon Counter



11 Software

- 11 Motion-Capture-Enabled Software for Gestural Control of 3D Models
- 11 Orbit Software Suite
- 11 CoNNeCT Baseband Processor Module Boot Code SoftWare (BCSW)
- 11 Trajectory Software With Upper Atmosphere Model
- 11 ALSSAT Version 6.0



13 Manufacturing & Prototyping

- 13 Employing a Grinding Technology to Assess the Microbial Density for Encapsulated Organisms
- 13 Demonstration of Minimally Machined Honeycomb Silicon Carbide Mirrors



15 Materials & Coatings

- 15 Polyimide Aerogel Thin Films
- 15 Nanoengineered Thermal Materials Based on Carbon Nanotube Array Composites
- 16 Composite Laminate With Coefficient of Thermal Expansion Matching D263 Glass



17 Mechanics/Machinery

- 17 Robust Tensioned Kevlar Suspension Design
- 17 Focal Plane Alignment Utilizing Optical CMM

19 Bio-Medical

- 19 Purifying, Separating, and Concentrating Cells From a Sample Low in Biomass
- 19 Virtual Ultrasound Guidance for Inexperienced Operators
- 20 Beat-to-Beat Blood Pressure Monitor



21 Physical Sciences

- 21 Non-Contact Conductivity Measurement for Automated Sample Processing Systems
- 21 An MSK Radar Waveform
- 22 Telescope Alignment From Sparsely Sampled Wavefront Measurements Over Pupil Subapertures
- 22 Method to Remove Particulate Matter From Dusty Gases at Low Pressures
- 23 Terahertz Quantum Cascade Laser With Efficient Coupling and Beam Profile
- 24 Measurement Via Optical Near-Nulling and Subaperture Stitching
- 25 885-nm Pumped Ceramic Nd:YAG Master Oscillator Power Amplifier Laser System



27 Books & Reports

- 27 Airborne Hyperspectral Imaging System
- 27 Heat Shield Employing Cured Thermal Protection Material Blocks Bonded in a Large-Cell Honeycomb Matrix
- 27 Asymmetric Supercapacitor for Long-Duration Power Storage

This document was prepared under the sponsorship of the National Aeronautics and Space Administration. Neither the United States Government nor any person acting on behalf of the United States Government assumes any liability resulting from the use of the information contained in this document, or warrants that such use will be free from privately owned rights.



Instrument Suite for Vertical Characterization of the Ionosphere-Thermosphere System

Goddard Space Flight Center, Greenbelt, Maryland

A document describes a suite that provides four simultaneous ion and neutral-atom measurements as a function of altitude, with variable sensitivity for neutral atmospheric species. The variable sensitivity makes it possible to extend the measurements over the altitude range of 100 to more than 700 km. The four instruments in the suite are (1) a neutral wind-temperature spectrometer (WTS), (2) an ion-drift ion-temperature spectrometer (IDTS), (3) a neutral mass spectrometer (NMS), and (4) an ion mass spectrometer (IMS).

The instrument suite has four sensors consisting of two different types of analyzers. The first two are energy-angle spectrometers: WTS for the wind-tem-

perature-O/N₂ ratio and IDTS for the ion drift-temperature-density ratios. The other two use a mass analyzer that allows two spectrometers to be combined into a single rectangular package, one-half for ions (IMS), the other for neutrals (NMS). The high payload velocity enables measurement of non-Maxwellian energy distributions, and also the separation of O from internal ion source products.

All instruments point in the same direction and require their common axis to point within 5° of the payload velocity vector to achieve the desired performance. In their simplest mode of operation, WTS and IDTS derive the component of the wind and ion-drift that is perpendicular to them. This is obtained

from the angle of the peak of the neutral (ion) flux passing the entrance aperture. The angular distribution of the particle flux appears on the detector plane. The line passing the aperture from outside represents the total velocity vector, the vector sum of the wind, and the payload velocity. Knowledge of the payload velocity coupled with precise knowledge of the peak plus the pointing of the WTS (IDTS) axis then yields the wind vector.

This work was done by Federico Herrero and Hollis Jones of Goddard Space Flight Center, and Theodore Finne and Andrew Nicholas of the Naval Research Laboratory. Further information is contained in a TSP (see page 1). GSC-15964-1

Terahertz Radiation Heterodyne Detector Using Two-Dimensional Electron Gas in a GaN Heterostructure

This detector has applications in spectroscopy of chemical species in atmospheres of planets, for detection of biochemical warfare agents, and terahertz imaging for port security.

NASA's Jet Propulsion Laboratory, Pasadena, California

High-resolution submillimeter/terahertz spectroscopy is important for studying atmospheric and interstellar molecular gaseous species. It typically uses heterodyne receivers where an unknown (weak) signal is mixed with a strong signal from the local oscillator (LO) operating at a slightly different frequency. The non-linear mixer devices for this frequency range are unique and are not off-the-shelf commercial products.

Three types of THz mixers are commonly used: Schottky diode, superconducting hot-electron bolometer (HEB), and superconductor-insulation-superconductor (SIS) junction. The latter two are the most sensitive and require very small LO power to be driven to the desired operating point. These mixers require deep cryogenic cooling to at least 4 K. Schottky mixers are less sensi-

tive and require stronger LO sources. However, they can be used at any ambient temperature.

A HEB mixer based on the two-dimensional electron gas (2DEG) formed at the interface of two slightly dissimilar semiconductors was developed. This mixer can operate at temperatures between 100 and 300 K, and thus can be used with just passive radiative cooling available even on small spacecraft. It requires small LO power (1–10 microwatt) and, therefore, can be driven by the existing LOs, even above 1 THz.

The mixer device is a micron-sized patch of the 2DEG formed in the AlInN/GaN heterostructure grown on sapphire substrate. The device operates as a bolometer with a temperature-dependent resistance (mobility of the 2DEG). Free electrons in the device ab-

sorb THz radiation received by a micro-antenna coupled to the mixer device. This changes the temperature of electrons and the bolometer resistance. The maximum speed of the mixer device of this type is set by the combination of the electron-phonon relaxation in the material and the diffusion of hot electrons through the device ends, and corresponds to several GHz. This is what is usually required for the intermediate frequency (IF) bandwidth of a typical THz mixer. One can say that this 2DEG HEB mixer combines the best qualities of the superconducting HEB mixer (low LO power, low noise) and of the Schottky-diode mixer (ambient temperature operation).

The main innovation here is the use of GaN-based heterostructures. Compared to the much better known GaAs-based heterostructures, the new material sys-

tem provides nearly ideal conditions for strong Drude absorption of radiation by electrons. This allows for the very short momentum relaxation time (time between collisions) of electrons. Since this time is shorter than a period of the THz field oscillation, the electrons absorb

THz radiation well. In the GaAs structures, the momentum relaxation time is usually much longer, so the electrons move in the field without collisions for a long time. This reduces their ability to absorb radiation and makes the mixer device much less sensitive.

This work was done by Boris S. Karasik, John J. Gill, Imran Mehdi, and Timothy J. Crawford of Caltech, and Andrei V. Sergeev and Vladimir V. Mitin of SUNY Buffalo for NASA's Jet Propulsion Laboratory. Further information is contained in a TSP (see page 1). NPO-47796

Pattern Recognition Algorithm for High-Sensitivity Odorant Detection in Unknown Environments

NASA's Jet Propulsion Laboratory, Pasadena, California

In a realistic odorant detection application environment, the collected sensory data is a mix of unknown chemicals with unknown concentrations and noise. The identification of the odorants among these mixtures is a challenge in data recognition. In addition, deriving their individual concentrations in the mix is also a challenge.

A deterministic analytical model was developed to accurately identify odorants and calculate their concentrations in a mixture with noisy data. This model is specially suited for hardware imple-

mentation with miniaturization. Hierarchical neural network architecture effectively deals with the induced odorants that can be formed from the combination of basic source odorants and their concentrations.

To search for an odorant in the mixture, where it exists in the operating environment, one of the most robust techniques is to recover the original odorant sources. When done, the detection can be an easy step by finding the minimum phase between the predicted original odorants and the target odorants. The

neural-network approach can be employed to capture the target odorants in various conditions through learning, i.e., concentration levels through the parameterized weight set, then the strongest correlation between parameterized weights and the predicted original can be used to identify the intended odorants.

This work was done by Tuan A. Duong of Caltech for NASA's Jet Propulsion Laboratory. For more information, contact iaoffice@jpl.nasa.gov. NPO-47485

Determining Performance Acceptability of Electrochemical Oxygen Sensors

This screening method does not affect the operation life of the sensor.

Lyndon B. Johnson Space Center, Houston, Texas

A method has been developed to screen commercial electrochemical oxygen sensors to reduce the failure rate. There are three aspects to the method: First, the sensitivity over time (several days) can be measured and the rate of change of the sensitivity can be used to predict sensor failure. This method has been demonstrated in ongoing tests. Second, an improvement to this method would be to store the sensors in an oxygen-free (e.g., nitrogen) environment and intermittently measure the sensitivity over time (several days) to accomplish the same result while preserving the sensor lifetime by limiting consumption of the electrode. Third, the second time derivative of the sensor response over time can be used to determine the point in time at which the sensors are sufficiently stable for use.

Commercial electrochemical oxygen sensors are a limited-lifetime item because

the sensor electrode is consumed during normal operation. Basically, a given sensor at the time of manufacture has a finite lifetime, which can be quantified in terms of ppm-hours so that an exposure to a given concentration for a given time reduces the lifetime by the product of those two factors. Common practice is to simply replace a sensor that fails within the vendor-specified lifetime. In applications requiring long operational life with no replacement option, screening of the sensors is advantageous to reduce the sensor failure rate. Prior art for screening is unknown given the commercial nature and application of these sensors. The simple and obvious method for screening would be to measure the sensor response at a known oxygen concentration (i.e., initial sensitivity) and determine a statistical threshold for excluding a sensor from use. However, this does not guarantee acceptable lifetime performance.

The benefits of the invention are reduced failure rate, which is especially advantageous in applications with long operational life requirements and no replacement option. In addition, this provides a screening method that does not affect the operation life of the sensor to accomplish this screening. Finally, the method provides a criterion for determining sensor acceptability prior to system level integration. These benefits significantly improve on the common practice, which cannot predict failure at any point in time beyond the initial screening. The oxygen-free environment method would prevent unnecessary reduction in the available lifetime of the sensor.

This work was done by Daniel Gonzales of Hamilton Sundstrand for Johnson Space Center. For further information, contact the JSC Innovation Partnerships Office at (281) 483-3809. MSC-24916-1

Versatile Controller for Infrared Lamp and Heater Arrays

NASA's Jet Propulsion Laboratory, Pasadena, California

A paper describes a modular design for new controllers for infrared heating during cruise stage solar thermal vacuum test of the Mars Science Laboratory. The controllers had to be easy to use and maintain, used with a wide variety of different control schemes, and made using commercial off-the-shelf (COTS) components wherever possible.

A new controller was designed and built using COTS components that could be operated manually, or automatically in a temperature control mode through the use of programmable PID (proportional-integral-deriva-

tive) controllers. Another option is through computer control to implement control schemes involving average over a number of sensors, with no sensor above or below the temperature set point or use of non-thermocouple sensors such as PRTs (platinum resistance thermometer), calorimeters, etc. The system incorporates a thermal failsafe to guard against high-temperature overruns of the test item, ground fault circuit interrupters for personal protection, and has provision for an external shutdown signal for other conditions such as a vacuum system entering the

corona region with the addition of a proper alarm system.

This controller was designed and built as a versatile general-purpose controller. Its modular design will make upgrades or modifications simple to implement. Previous controllers used at JPL were purpose-built for the project that required them, and difficult to upgrade or modify.

This work was done by Michael R. McKee, Isaac M. Brown, Seth L. Chazanoff, and Bruce Woodward of Caltech for NASA's Jet Propulsion Laboratory. Further information is contained in a TSP (see page 1). NPO-47402

High-Speed Scanning Interferometer Using CMOS Image Sensor and FPGA Based on Multifrequency Phase-Tracking Detection

Applications include LCD/plasma display inspection and semiconductor wafer process characterization.

Goddard Space Flight Center, Greenbelt, Maryland

A sub-aperture stitching optical interferometer can provide a cost-effective solution for an *in situ* metrology tool for large optics; however, the currently available technologies are not suitable for high-speed and real-time continuous scan. NanoWave's SPPE (Scanning Probe Position Encoder) has been proven to exhibit excellent stability and sub-nanometer precision with a large dynamic range. This same technology can transform many optical interferometers into real-time subnanometer precision tools with only minor modification.

The proposed field-programmable gate array (FPGA) signal processing concept, coupled with a new-generation, high-speed, mega-pixel CMOS (comple-

mentary metal-oxide semiconductor) image sensor, enables high speed (>1 m/s) and real-time continuous surface profiling that is insensitive to variation of pixel sensitivity and/or optical transmission/reflection. This is especially useful for large optics surface profiling.

Due to the patented phase synchronous tracking detection scheme in the time domain, the new method has already demonstrated better than 65 pm rms measurement noise (from single-pixel information alone) using an experimental setup, while up to 60 pm dynamic phase accuracy over the entire measurement range is predicted. Simulation shows that the measurement noise level could reach 1–2 pm.

It also correctly maps the phase even when high-density fringe is present under faint light condition (similar to lock-in amplifier). The real-time scanning also provides sub-pixel spatial resolution. This new technology is capable of measuring steep wall objects or aspheres with more than a few hundred waves of aspheric departure without the use of dedicated null lenses or computer-generated holograms. Thus, a compact, scalable, low-cost and low-energy consumption system can be achieved.

This work was done by Tetsuo Ohara of Goddard Space Flight Center. Further information is contained in a TSP (see page 1). GSC-15942-1

Ultra-Low-Power MEMS Selective Gas Sensors

Sensor uses 10 to 1,000 times less power than current commercial sensors.

John H. Glenn Research Center, Cleveland, Ohio

This innovation is a system for gas sensing that includes an ultra-low-power MEMS (microelectromechanical system) gas sensor, combined with

unique electronic circuitry and a proprietary algorithm for operating the sensor. The electronics were created from scratch, and represent a novel de-

sign capable of low-power operation of the proprietary MEMS gas sensor platform. The algorithm is used to identify a specific target gas in a gas mixture,

making the sensor selective to that target gas.

The objectives achieved include the development of an ultra-low-power, low-cost, high-performance, selective MEMS gas sensor for cryogenic and energy gases, such as H₂, He, CH₄, and CO₂. This product will have unique competitive advantages over current offerings because it uses 10 to 1,000 times less power than current commercial sensors, enabling low-cost distributed sensing in a wide variety of NASA and private sector applications. This sensor is also highly reliable, ultra-stable, and selective to single gases in mixtures, creating a combination of features that cannot be matched with other state-of-the-art technologies. Many proprietary and non-pro-

prietary gas sensor technologies exist to monitor energy gases, each with their own advantages and disadvantages. However, none of these technologies or methods operates at the low power of this MEMS gas sensor, with selectivity, long-term stability, and reliability over a long period of time.

Novel and unique features include the new nano-TCD sensor platform; ultra-low-power operation (<10 nanowatt per reading), fast response (measured in nanoseconds, >1,000 times faster than current devices, and stability through tens of billions of measurements and over environmental temperature and RH ranges, and calibration stability for >5 years with no consumables and unprecedented selectivity. The pro-

prietary software is original and does not reuse existing code, shareware, or code owned by a non-federal entity. The algorithm developed is the novel element added to the patented nano-TCD structure and is proprietary.

This work was done by Joseph Stetter of KWJ Engineering, Inc. for Glenn Research Center. Further information is contained in a TSP (see page 1).

Inquiries concerning rights for the commercial use of this invention should be addressed to NASA Glenn Research Center, Innovative Partnerships Office, Attn: Steven Fedor, Mail Stop 4-8, 21000 Brookpark Road, Cleveland, Ohio 44135. Refer to LEW-18831-1.



Compact Receiver Front Ends for Submillimeter-Wave Applications

NASA's Jet Propulsion Laboratory, Pasadena, California

The current generation of submillimeter-wave instruments is relatively mass- and power-hungry. The receiver front ends (RFEs) of a submillimeter instrument form the heart of the instrument, and any mass reduction achieved in this subsystem is propagated through the instrument. In the current implementation, the RFE consists of different blocks for the mixer and LO circuits. The motivation for this work is to reduce the mass of the RFE by integrating the mixer and LO circuits in one waveguide block.

The mixer and its associated LO chips will all be packaged in a single waveguide package. This will reduce the mass of the RFE and also provide a number of other advantages. By bringing the mixer and LO circuits close together, losses in the waveguide will be reduced. More-

over, the compact nature of the block will allow for better thermal control of the block, which is important in order to reduce gain fluctuations.

A single waveguide block with a 600-GHz RFE functionality (based on a subharmonically pumped Schottky diode pair) has been demonstrated. The block is about $3 \times 3 \times 3$ cm³. The block combines the mixer and multiplier chip in a single package. 3D electromagnetic simulations were carried out to design the waveguide circuit around the mixer and multiplier chip. The circuit is optimized to provide maximum output power and maximum bandwidth.

An integrated submillimeter front end featuring a 520–600-GHz sub-harmonic mixer and a 260–300-GHz frequency tripler in a single cavity was

tested. Both devices used GaAs MMIC membrane planar Schottky diode technology. The sub-harmonic mixer/tripler circuit has been tested using conventional metal-machined blocks. Measurement results on the metal block give best DSB (double sideband) mixer noise temperature of 2,360 K and conversion losses of 7.7 dB at 520 GHz. The LO input power required to pump the integrated tripler/sub-harmonic mixer is between 30 and 50 mW.

This work was done by Imran Mehdi, Goutam Chattopadhyay, Erich T. Schlecht, Robert H. Lin, Seth Sin, Alejandro Peralta, Choonsup Lee, John J. Gill, Samuel Gulkis, and Bertrand C. Thomas of Caltech for NASA's Jet Propulsion Laboratory. For more information, contact iaoffice@jpl.nasa.gov. NPO-47902

Dynamically Reconfigurable Systolic Array Accelerator

Goddard Space Flight Center, Greenbelt, Maryland

A polymorphic systolic array framework has been developed that works in conjunction with an embedded microprocessor on a field-programmable gate array (FPGA), which allows for dynamic and complimentary scaling of acceleration levels of two algorithms active concurrently on the FPGA. Use is made of systolic arrays and a hardware-software co-design to obtain an efficient multi-ap-

plication acceleration system. The flexible and simple framework allows hosting of a broader range of algorithms, and is extendable to more complex applications in the area of aerospace embedded systems.

FPGA chips can be responsive to real-time demands for changing applications' needs, but only if the electronic fabric can respond fast enough. This systolic array

framework allows for rapid partial and dynamic reconfiguration of the chip in response to the real-time needs of scalability, and adaptability of executables.

This work was done by Aravind Dasu and Robert Barnes of Utah State University Research for Goddard Space Flight Center. For further information, contact the Goddard Innovative Partnerships Office at (301) 286-5810. GSC-16303-1

Blocking Losses With a Photon Counter

Losses for single detectors and arrays of detectors are characterized.

NASA's Jet Propulsion Laboratory, Pasadena, California

It was not known how to assess accurately losses in a communications link due to photodetector blocking, a phenomenon wherein a detector is rendered inactive for a short time after the detection of a photon. When used to detect a communications signal, blocking

leads to losses relative to an ideal detector, which may be measured as a reduction in the communications rate for a given received signal power, or an increase in the signal power required to support the same communications rate. This work involved characterizing block-

ing losses for single detectors and arrays of detectors.

Blocking may be mitigated by spreading the signal intensity over an array of detectors, reducing the count rate on any one detector. A simple approximation was made to the blocking loss as a

function of the probability that a detector is unblocked at a given time, essentially treating the blocking probability as a scaling of the detection efficiency.

An exact statistical characterization was derived for a single detector, and an approximation for multiple detectors. This allowed derivation of several accurate approximations to the loss. Methods were also derived to account for a rise time in recovery, and non-uniform illumination due to diffraction and atmospheric distortion of the phase front.

It was assumed that the communications signal is intensity modulated and received by an array of photon-counting

photodetectors. For the purpose of this analysis, it was assumed that the detectors are ideal, in that they produce a signal that allows one to reproduce the arrival times of electrons, produced either as photoelectrons or from dark noise, exactly. For single detectors, the performance of the maximum-likelihood (ML) receiver in blocking is illustrated, as well as a maximum-count (MC) receiver, that, when receiving a pulse-position-modulated (PPM) signal, selects the symbol corresponding to the slot with the largest electron count.

Whereas the MC receiver saturates at high count rates, the ML receiver may

not. The loss in capacity, symbol-error-rate (SER), and count-rate were numerically computed. It was shown that the capacity and symbol-error-rate losses track, whereas the count-rate loss does not generally reflect the SER or capacity loss, as the slot-statistics at the detector output are no longer Poisson. It is also shown that the MC receiver loss may be accurately predicted for dead times on the order of a slot.

This work was done by Bruce E. Moision and Sabino Piazzolla of Caltech for NASA's Jet Propulsion Laboratory. For more information, contact iaoffice@jpl.nasa.gov. NPO-48411



Motion-Capture-Enabled Software for Gestural Control of 3D Models

Current state-of-the-art systems use general-purpose input devices such as a keyboard, mouse, or joystick that map to tasks in unintuitive ways. This software enables a person to control intuitively the position, size, and orientation of synthetic objects in a 3D virtual environment. It makes possible the simultaneous control of the 3D position, scale, and orientation of 3D objects using natural gestures.

Enabling the control of 3D objects using a commercial motion-capture system allows for natural mapping of the many degrees of freedom of the human body to the manipulation of the 3D objects. It reduces training time for this kind of task, and eliminates the need to create an expensive, special-purpose controller.

This work was done by Jeffrey S. Norris, Victor Luo, Thomas M. Crockett, Khawaja S. Shams, and Mark W. Powell of Caltech; and Anthony Valderrama of MIT for NASA's Jet Propulsion Laboratory. Further information is contained in a TSP (see page 1).

This software is available for commercial licensing. Please contact Daniel Broderick of the California Institute of Technology at danielb@caltech.edu. Refer to NPO-47893.

Orbit Software Suite

Orbit Software Suite is used to support a variety of NASA/DM (Dependable Multiprocessor) mission planning and analysis activities on the IPS (Intrusion Prevention System) platform. The suite of Orbit software tools (Orbit Design and Orbit Dynamics) resides on IPS/Linux workstations, and is used to perform mission design and analysis tasks corresponding to trajectory/launch window, rendezvous, and proximity operations flight segments. A list of tools in Orbit Software Suite represents tool versions established during/after the Equipment Rehost-3 Project.

This work was done by Cathy Osgood, Kevin Williams, Philip Gentry, Dana Brownfield, John Hallstrom, and Tim Stuit of United Space Alliance for Johnson Space Center. For further information, contact the JSC Innovation Partnerships Office at (281) 483-3809. MSC-24956-1

CoNNeCT Baseband Processor Module Boot Code Software (BCSW)

This software provides essential start-up and initialization routines for the CoNNeCT baseband processor module (BPM) hardware upon power-up. A command and data handling (C&DH) interface is provided via 1553 and diagnostic serial interfaces to invoke operational, reconfiguration, and test commands within the code.

The BCSW has features unique to the hardware it is responsible for managing. In this case, the CoNNeCT BPM is configured with an updated CPU (Atmel AT697 SPARC processor) and a unique set of memory and I/O peripherals that require customized software to operate. These features include configuration of new AT697 registers, interfacing to a new HouseKeeper with a flash controller interface, a new dual Xilinx configuration/scrub interface, and an updated 1553 remote terminal (RT) core.

The BCSW is intended to provide a "safe" mode for the BPM when initially powered on or when an unexpected trap occurs, causing the processor to reset. The BCSW allows the 1553 bus controller in the spacecraft or payload controller to operate the BPM over 1553 to upload code; upload Xilinx bit files; perform rudimentary tests; read, write, and copy the non-volatile flash memory; and configure the Xilinx interface. Commands also exist over 1553 to cause the CPU to jump or call a specified address to begin execution of user-supplied code. This may be in the form of a real-time operating system, test routine, or specific application code to run on the BPM.

This work was done by Clifford K. Yamamoto, David S. Orozco, D. J. Byrne, Steven J. Allen, Adit Sahasrabudhe, and Minh Lang of Caltech for NASA's Jet Propulsion Laboratory. Further information is contained in a TSP (see page 1).

This software is available for commercial licensing. Please contact Daniel Broderick of the California Institute of Technology at danielb@caltech.edu. Refer to NPO-47778.

Trajectory Software With Upper Atmosphere Model

The Trajectory Software Applications 6.0 for the Dec Alpha platform has an im-

plementation of the Jacchia-Lineberry Upper Atmosphere Density Model used in the Mission Control Center for International Space Station support. Previous trajectory software required an upper atmosphere to support atmosphere drag calculations in the Mission Control Center. The Functional operation will differ depending on the end-use of the module.

In general, the calling routine will use function-calling arguments to specify input to the processor. The atmosphere model will then compute and return atmospheric density at the time of interest.

This program was written by Charles Barrett of United Space Alliance, Flight Design and Dynamics, for Johnson Space Center. For further information, contact the JSC Innovation Partnerships Office at (281) 483-3809. MSC-24250-1

ALSSAT Version 6.0

Advanced Life Support Sizing Analysis Tool (ALSSAT) at the time of this reporting has been updated to version 6.0. A previous version was described in "Tool for Sizing Analysis of the Advanced Life Support System" (MSC-23506), *NASA Tech Briefs*, Vol. 29, No. 12 (December 2005), page 43. To recapitulate: ALSSAT is a computer program for sizing and analyzing designs of environmental-control and life-support systems for spacecraft and surface habitats to be involved in exploration of Mars and the Moon. Of particular interest for analysis by ALSSAT are conceptual designs of advanced life-support (ALS) subsystems that utilize physicochemical and biological processes to recycle air and water and process human wastes to reduce the need of resource resupply.

ALSSAT is a means of investigating combinations of such subsystems' technologies featuring various alternative conceptual designs and thereby assisting in determining which combination is most cost-effective. ALSSAT version 6.0 has been improved over previous versions in several respects, including the following additions: an interface for reading sizing data from an ALS database, computational models of a redundant regenerative CO₂ and Moisture Removal Amine Swing Beds (CAMRAS) for CO₂ removal, upgrade of the Temperature & Humidity Control's Common

Cabin Air Assembly to a detailed sizing model, and upgrade of the Food-management subsystem.

This work was done by Hue-Hsia (Jan-nivine) Yeh and Cheryl Brown of Hamilton Sundstrand Corp., and Frank Jeng of Barrios

Technology for Johnson Space Center. Further information is contained in a TSP (see page 1). MSC-24355-1



Employing a Grinding Technology to Assess the Microbial Density for Encapsulated Organisms

Applications include medical device manufacturing and the commercial paint industry.

NASA's Jet Propulsion Laboratory, Pasadena, California

Projects that utilize large volumes of nonmetallic materials of planetary protection concern pose a challenge to their bioburden budget, as the most conservative value of 30 spores/cm³ is typically used. The standard laboratory procedures do not provide any direction into the methodologies to understand the embedded bioburden within such nonmetallic components such as adhesives, insulation, or paint. A project can elect to conduct a destructive hardware study to experimentally derive a source-specific encapsulated microbial density, and the experimental value can be utilized for a project.

A tailored, novel, destructive hardware technology employing a household box grater was developed to assess the embedded bioburden within the adhesives, insulation, and paint for the Mars Science Laboratory (MSL) project.

Similar technologies used for the destructive analyses of nonmetallic components include chemical/solvent-based methods, blenders, mortar and pestle crushing, French press, pulverizing, and bead beating methods. These similar technologies are typically lethal to viable biological cells due to the excess generation of heat or adverse chemical



The Box Grater (left), and the size of Cured Paint Particles that were generated upon grating (right).

interactions that render cells non-viable. These typical destructive hardware methodologies proved ineffective in breaking up the material into suitable size particles due to the material composition of the adhesives, insulation, and paint. Therefore, a novel approach had to be devised.

Samples were placed on a sterile tray and cut into three 5×5 cm pieces. The cut piece was wiped with a sterile wipe and 2-propanol. The cleaned material was then grated gently on the smallest grading plane on the box grater into sugar-crystal-sized pieces. The box grater approach is advantageous due to the ease and ability

of the entire system to be sterilized, minimal (or negligible) impact to recontamination if performed in a Class 100 flow bench, and controllable heat generation upon material destruction. The recovery percentages of spores seeded on flight or surrogate materials were <10% for surrogate and <50% for flight, and could be applicable along with other chemical or physical technologies.

This work was done by James N. Benardini, Fabian Morales, Wayne W. Schubert, Gayane A. Kazarians, and Robert C. Koukol of Caltech for NASA's Jet Propulsion Laboratory. Further information is contained in a TSP (see page 1). NPO-48299

Demonstration of Minimally Machined Honeycomb Silicon Carbide Mirrors

This manufacturing process eliminates machining and steps for mirrors and optomechanical structures.

Marshall Space Flight Center, Alabama

Honeycomb silicon carbide composite mirrors are made from a carbon fiber preform that is molded into a honeycomb shape using a rigid mold. The carbon fiber honeycomb is densified by using polymer infiltration pyrolysis, or through a reaction with liquid silicon. A chemical vapor deposit, or chemical

vapor composite (CVC), process is used to deposit a polishable silicon or silicon carbide cladding on the honeycomb structure. Alternatively, the cladding may be replaced by a freestanding, replicated CVC SiC facesheet that is bonded to the honeycomb. The resulting carbon fiber-reinforced silicon carbide honey-

comb structure is a ceramic matrix composite material with high stiffness and mechanical strength, high thermal conductivity, and low CTE (coefficient of thermal expansion). This innovation enables rapid, inexpensive manufacturing.

The web thickness of the new material is less than 1 mm, and core geometries

(pocket depth, pocket size) are easily tailored. These parameters are based on precursor carbon-carbon honeycomb material made and patented by Ultracor. It is estimated at the time of this reporting that the HoneySiC™ will have a net production cost on the order of \$38,000/m². This includes an Ultracor raw material cost of about \$97,000/m², and a Trex silicon carbide deposition cost of \$27,000/m². Even at double this price, HoneySiC would beat NASA's goal of \$100,000/m². Cost savings are estimated to be 40 to 100 times that of current mirror technologies.

The organic, rich prepreg material has a density of 56 kg/m³. A charred carbon-carbon panel (volatile organics

burnt off) has a density of 270 kg/m³. Therefore, it is estimated that a HoneySiC panel would have a density of no more than 900 kg/m³, which is about half that of beryllium and about one-third the density of bulk silicon carbide. It is also estimated that larger mirrors could be produced in a matter of weeks.

Each cell is completely uniform, maintaining the shape of the inserted mandrel. Furthermore, the layup creates pressure that insures node bond strength. Each node is a composite laminate using only the inherent resin system to form the bond. This contrasts starkly with the other known method of producing composite honeycomb, in

which individual corrugations are formed, cured, and then bonded together in a secondary process.

By varying the size of the mandrels within the layup, varying degrees of density can be achieved. Typical sizes are 3/8 and 3/16 in. (≈10 and 5 mm). Cell sizes up to 1 in. (≈25 mm) have been manufactured. Similarly, the shape of the core can be altered for a flexible honeycomb structure.

This work was done by William Goodman of Trex Enterprises Corporation for Marshall Space Flight Center. For more information, contact Sammy Nabors, MSFC Commercialization Assistance Lead, at sammy.a.nabors@nasa.gov. Refer to MFS-32866-1.



Polyimide Aerogel Thin Films

John H. Glenn Research Center, Cleveland, Ohio

Polyimide aerogels have been cross-linked through multifunctional amines. This invention builds on “Polyimide Aerogels With Three-Dimensional Cross-Linked Structure,” (LEW-18486-1), *NASA Tech Briefs*, Vol. 34, No. 8 (August 2010), page 38, and may be considered as a continuation of that invention, which results in a polyimide aerogel with a flexible, formable form.

Gels formed from polyamic acid solutions, end-capped with anhydrides, and

cross-linked with the multifunctional amines, are chemically imidized and dried using supercritical CO₂ extraction to give aerogels having density around 0.1 to 0.3 g/cm³. The aerogels are 80 to 95% porous, and have high surface areas (200 to 600 m²/g) and low thermal conductivity (as low as 14 mW/m-K at room temperature). Notably, the cross-linked polyimide aerogels have higher modulus than polymer-reinforced silica aerogels of similar density,

and can be fabricated as both monoliths and thin films.

This work was done by Mary Ann Meador of Glenn Research Center and Haiquan Guo of Ohio Aerospace Institute. Further information is contained in a TSP (see page 1).

Inquiries concerning rights for the commercial use of this invention should be addressed to NASA Glenn Research Center, Innovative Partnerships Office, Attn: Steven Fedor, Mail Stop 4-8, 21000 Brookpark Road, Cleveland, Ohio 44135. Refer to LEW-18864-1.

Nanoengineered Thermal Materials Based on Carbon Nanotube Array Composites

Thermal conductors for integrated circuits and devices can be made from carbon nanotube arrays.

Ames Research Center, Moffett Field, California

State-of-the-art integrated circuits (ICs) for microprocessors routinely dissipate power densities on the order of 50 W/cm². This large power is due to the localized heating of ICs operating at high frequencies and must be managed for future high-frequency microelectronic applications. As the size of components and devices for ICs and other appliances becomes smaller, it becomes more difficult to provide heat dissipation and transport for such components and devices. A thermal conductor for a macro-sized thermal conductor is generally inadequate for use with a micro-sized component or device, in part due to scaling problems.

The cooling of an object by attaching it to a cold reservoir is normally limited by the heat transfer rate across the interface. Except for objects with atomically flat surfaces, practical objects normally have only a very small portion of surface in contact with other solid surfaces. Eutectic bonding materials or thermal conducting pastes/films are normally applied at the interface to increase the contact area. However, the thermal conductivities of these eutectic bonding materials are normally an order of magnitude lower than

those of solid materials such as Cu and Si. The interface thus remains the bottleneck for heat dissipation.

A method has been developed for providing for thermal conduction using an array of carbon nanotubes (CNTs). An array of vertically oriented CNTs is grown on a substrate having high thermal conductivity, and interstitial regions between adjacent CNTs in the array are partly or wholly filled with a filler material having a high thermal conductivity so that at least one end of each CNT is exposed. The exposed end of each CNT is pressed against a surface of an object from which heat is to be removed. The CNT-filler composite adjacent to the substrate provides improved mechanical strength to anchor CNTs in place, and also serves as a heat spreader to improve diffusion of heat flux from the smaller volume (CNTs) to a larger heat sink.

The invention uses an embedded carbon nanotube array to provide one or more high-performance thermal conductors for applications that require large heat dissipation. This approach also improves the mechanical strength of carbon nanotubes (CNTs) so that the CNT array can remain stable and make

good contact to the surface of objects that generate a large amount of heat, through use of reversible buckling and bending of exposed portions of the CNTs. The extremely high thermal conductivity along a carbon nanotube axis is employed to transfer heat away from hot spots in a component or device. Copper and other high-thermal-conductivity materials are deposited to fill interstitial regions or gaps in the first part of a CNT array.

The fabrication involves four steps: (1) Substantially vertically aligned CNT arrays with a preferred length of from 1 to 50 microns are grown on a solid substrate (serving as a heat sink) that has good thermal conductivity, such as Si wafers and metal blocks/films; (2) a first portion of, or all of, interstitial spaces between adjacent CNTs are filled with high-thermal-conductivity materials such as Cu, Ag, Au, Pt, or doped Si by chemical vapor deposition (CVD), physical vapor deposition (PVD), plasma deposition, ion sputtering, electrochemical deposition, or casting from liquid phase; (3) filler materials are removed from a second portion of the interstitial spaces by mechanical polishing (MP),

chemical mechanical polishing (CMP), wet chemical etching, electrochemical etching, or dry plasma etching so that the top portion of the CNT array is exposed, with the bottom part remaining embedded in the filler materials; and (4) the embedded CNT array is applied against an object that is to be cooled. CNTs can reversibly buckle or bend one-by-one under low loading pressure so that a CNT can make maximum contact

with the object to be cooled, even an object with a very rough surface.

Heat can be effectively transferred from the contacting spots along the tube axis to the filler materials as well as the substrates. The filler materials play two critical roles: improving the mechanical stability and maximizing the thermal conductivity. Choosing highly thermal conductive materials as the filler matrix maximizes the heat transfer from the contact spots to the

substrate (i.e., the heat sink or cooling reservoir). An embedded CNT array can be reused without damage or compromise of its heat transport characteristics, in contrast to an approach that relies upon eutectic bonding.

This work was done by Jun Li and Meyya Meyyappan of Ames Research Center, and Carlos Dangelo of QSolis Inc. Further information is contained in a TSP (see page 1). ARC-15173-1

Composite Laminate With Coefficient of Thermal Expansion Matching D263 Glass

The laminate is a combination of carbon fiber with fiberglass.

Goddard Space Flight Center, Greenbelt, Maryland

The International X-ray Observatory project seeks to make an X-ray telescope assembly with 14,000 flexible glass segments. The glass used is commercially available SCHOTT D263 glass. Thermal expansion causes the mirror to distort out of alignment. A housing material is needed that has a matching coefficient of thermal expansion (CTE) so that when temperatures change in the X-ray mirror assembly, the glass and housing pieces expand equally, thus reducing or eliminating distortion. Desirable characteristics of this material include a high stiffness/weight ratio, and low density.

Some metal alloys show promise in matching the CTE of D263 glass, but their density is high compared to aluminum, and their stiffness/weight ratio is not favorable. A laminate made from carbon fiber reinforced plastic (CFRP) should provide more favorable

characteristics, but there has not been any made with the CTE matching D263 Glass.

It is common to create CFRP laminates of various CTEs by stacking layers of "prepreg" material at various angles. However, the CTE of D263 glass is 6.3 ppm/°C at 20 °C, which is quite high, and actually unachievable solely with carbon fiber and resin.

A composite laminate has been developed that has a coefficient of thermal expansion identical to that of SCHOTT D263 glass. The laminate is made of a combination of T300 carbon fiber, E-glass, and RS3C resin. The laminate has 50% uni-T300 plies and 50% uni-E-glass plies, with each fiber-layer type laid up in a quasi-isotropic laminate for a total of 16 plies. The fiber volume (percent of fiber compared to the resin) controls the CTE to a great extent. Tests have con-

firmed that a fiber volume around 48% gives a CTE of 6.3 ppm/°C. This is a fairly simple composite laminate, following well established industry procedures.

The unique feature of this laminate is a somewhat unusual combination of carbon fiber with E-glass (fiberglass). The advantage is that the resulting CTE comes out to 6.3 ppm/°C at 20 °C, which matches D263 glass. The trick with this laminate is to establish the proper fiber volume to get the desired CTE. Laminates were made with several different fiber volumes and coupons were tested to establish the relationship between fiber volume and CTE. Testing proved that fiber volume should be about 48%.

This work was done by David Robinson and Benjamin Rodini of Goddard Space Flight Center. Further information is contained in a TSP (see page 1). GSC-16261-1



⚙️ Robust Tensioned Kevlar Suspension Design

A suite of compact design elements improves the reliability of Kevlar suspension systems.

NASA's Jet Propulsion Laboratory, Pasadena, California

One common but challenging problem in cryogenic engineering is to produce a mount that has excellent thermal isolation but is also rigid. Such mounts can be achieved by suspending the load from a network of fibers or strings held in tension. Kevlar fibers are often used for this purpose owing to their high strength and low thermal conductivity. However, Kevlar presents challenges since it expands on cooling and tends to creep after initial tensioning, causing reductions in the resonant frequencies and a shift in the position of the suspended element, which can lead to misalignment and thermal short circuits. With existing designs, such as the Kevlar suspension used on the Herschel SPIRE instrument, it is difficult to re-tension the Kevlar or measure the tension because parts of the Kevlar string are staked with epoxy. Non-cryogenic designs used on a larger scale,

such as tensioning reels on sailboats, use turnbuckles and fixed eyebolts that cannot be scaled down to a small-scale structure without a significant addition of mass.

A suite of compact design elements has been developed to improve the reliability of suspension systems made of Kevlar. The Kevlar is anchored to the load via a pair of tensioning stars whose arm stiffness is optimized to ensure that the Kevlar spans remain sufficiently taut during and after thermal cycling. All other anchor points for the Kevlar are designed to have much higher stiffness to maintain the optimal geometry when under load. Pulleys are used at each anchor point allowing the tension to equalize between all spans. The resulting symmetry allows the load to remain fixed in space even as the suspension elements undergo thermal strain, and the tension buffering provided by the tensioning

stars reduces the concomitant changes in the structure's resonant frequencies.

The tension is adjusted by means of a capstan made of an array of stainless steel dowel pins to which the Kevlar string is belayed. Each pin has a large diameter compared to the Kevlar string so there are no machined corners that might initiate fraying of the Kevlar. The capstan is locked with an integrated mechanical clamp, so no epoxy is needed to secure the Kevlar or the capstan in place. Thus, the tension of the Kevlar can be adjusted after the initial creep or easily reworked if needed. The tension can be measured in situ by measuring the flexure of a single arm of the tensioning star.

This work was done by Joseph B. Young, Bret J. Naylor, and Warren A. Holmes of Caltech for NASA's Jet Propulsion Laboratory. Further information is contained in a TSP (see page 1). NPO-47940

⚙️ Focal Plane Alignment Utilizing Optical CMM

This approach will eliminate all requirements on positional tolerances.

NASA's Jet Propulsion Laboratory, Pasadena, California

In many applications, an optical detector has to be located relative to mechanical reference points. One solution is to specify stringent requirements on (1) mounting the optical detector relative to the chip carrier, (2) soldering the chip carrier onto the printed circuit board (PCB), and (3) installing the PCB to the mechanical structure of the subsystem. Figure 1 shows a sketch of an optical detector mounted relative to mechanical reference with high positional accuracy. The optical detector is typically a fragile wafer that cannot be physically touched by any measurement tool.

An optical coordinate measuring machine (CMM) can be used to position optical detectors relative to mechanical reference points. This approach will eliminate all requirements on positional

tolerances. The only requirement is that the PCB is manufactured with oversized holes. An exaggerated sketch of this situ-

ation is shown in Figure 2. The sketch shows very loose tolerances on mounting the optical detector in the chip car-

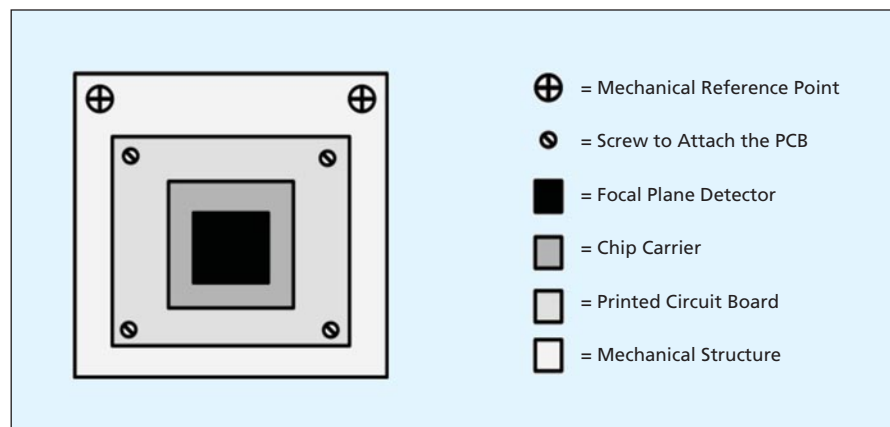


Figure 1. Sketch of an Optical Detector.

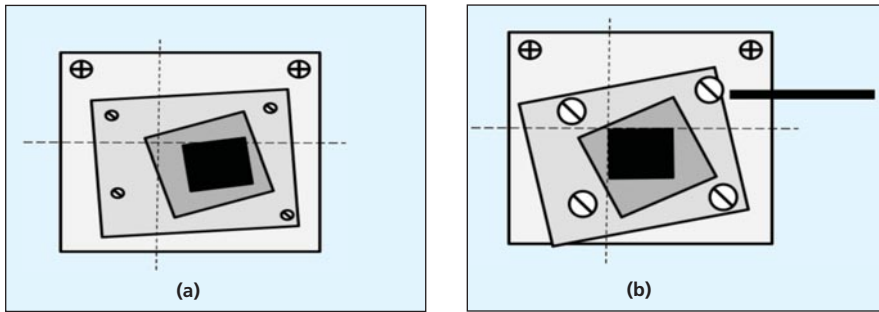


Figure 2. The **Optical CMM Measures the Mechanical Reference Points**. (a) Cross hairs indicate where the detector is supposed to be. (b) The PCB is tapped around until the corner of the optical detector is at the crosshairs of the CMM.

rier, loose tolerance on soldering the chip carrier to the PCB, and finally large tolerance on where the mounting screws are located. The PCB is held with large screws and oversized holes.

The PCB is mounted loosely so it can move freely around. The optical CMM measures the mechanical reference points. Based on these measurements, the required positions of the optical detector corners can be calculated. The

optical CMM is commanded to go to the position where one detector corner is supposed to be. This is indicated with the crosshairs in Figure 2(a). This figure is representative of the image of the optical CMM monitor. Using a suitable tapping tool, the PCB is manually tapped around until the corner of the optical detector is at the crosshairs of the optical CMM. The CMM is commanded to another corner, and the process is re-

peated a number of times until all corners of the optical detector are within a distance of 10 to 30 microns of the required position. The situation is sketched in Figure 2(b) (the figure also shows the tapping tool and where to tap). At this point the fasteners for the PCB are torqued slightly so the PCB can still move. The PCB location is adjusted again with the tapping tool. This process is repeated 3 to 4 times until the final torque is achieved. The oversized mounting holes are then filled with a liquid bonding agent to secure the board in position (not shown in the sketch). A 10- to 30-micron mounting accuracy has been achieved utilizing this method.

This work was done by Carl Christian Liebe, Patrick L. Meras, Gerald J. Clark, Jack J. Sedaka, Joel V. Kaluzny, and Brian Hirsch of Caltech; Todd A. Decker of Calwest Engineering; and Christopher R. Scholz of the University of California Berkeley for NASA's Jet Propulsion Laboratory. For more information, contact iaoffice@jpl.nasa.gov. NPO-47846



Purifying, Separating, and Concentrating Cells From a Sample Low in Biomass

This fluorescence-activated cell-sorting-based approach has applications in operating room cleanliness validation assays, and in pharmaceutical development and quality assurance.

NASA's Jet Propulsion Laboratory, Pasadena, California

Frequently there is an inability to process and analyze samples of low biomass due to limiting amounts of relevant biomaterial in the sample. Furthermore, molecular biological protocols geared towards increasing the density of recovered cells and biomolecules of interest, by their very nature, also concentrate unwanted inhibitory humic acids and other particulates that have an adversarial effect on downstream analysis.

A novel and robust fluorescence-activated cell-sorting (FACS)-based technology has been developed for purifying (removing cells from sampling matrices), separating (based on size, density, morphology), and concentrating cells (spores, prokaryotic, eukaryotic) from a sample low in biomass.

The technology capitalizes on fluorescent cell-sorting technologies to purify and concentrate bacterial cells from a low-biomass, high-volume sample. Over the past decade, cell-sorting detection systems have undergone enhancements and increased sensitivity, making bacterial cell sorting a feasible concept. Although there are many unknown limitations with regard to the applicability of this technology to environmental samples (smaller

cells, few cells, mixed populations), dogmatic principles support the theoretical effectiveness of this technique upon thorough testing and proper optimization. Furthermore, the pilot study from which this report is based proved effective and demonstrated this technology capable of sorting and concentrating bacterial endospore and bacterial cells of varying size and morphology.

Two commercial off-the-shelf bacterial counting kits were used to optimize a bacterial stain/dye FACS protocol. A LIVE/DEAD BacLight Viability and Counting Kit was used to distinguish between the live and dead cells. A Bacterial Counting Kit comprising SYTO BC (mixture of SYTO dyes) was employed as a broad-spectrum bacterial counting agent. Optimization using epifluorescence microscopy was performed with these two dye/stains. This refined protocol was further validated using varying ratios and mixtures of cells to ensure homogenous staining compared to that of individual cells, and were utilized for flow analyzer and FACS labeling.

This technology focuses on the purification and concentration of cells from

low-biomass spacecraft assembly facility samples. Currently, purification and concentration of low-biomass samples plague planetary protection downstream analyses. Having a capability to use flow cytometry to concentrate cells out of low-biomass, high-volume spacecraft/facility sample extracts will be of extreme benefit to the fields of planetary protection and astrobiology.

Successful research and development of this novel methodology will significantly increase the knowledge base for designing more effective cleaning protocols, and ultimately lead to a more empirical and "true" account of the microbial diversity present on spacecraft surfaces. Refined cleaning and an enhanced ability to resolve microbial diversity may decrease the overall cost of spacecraft assembly and/or provide a means to begin to assess challenging planetary protection missions.

This work was done by James N. Bernardini, Myron T. La Duc, and Rochelle Diamond of Caltech for NASA's Jet Propulsion Laboratory. Further information is contained in a TSP (see page 1). NPO-48086

Virtual Ultrasound Guidance for Inexperienced Operators

This audio/video system provides real-time help to inexperienced ultrasound operators in remote environments.

Lyndon B. Johnson Space Center, Houston, Texas

Medical ultrasound or echocardiographic studies are highly operator-dependent and generally require lengthy training and internship to perfect. To obtain quality echocardiographic images in remote environments, such as on-orbit, remote guidance of studies has been employed. This technique involves minimal training for the user, coupled with remote guidance from an expert. When real-time

communication or expert guidance is not available, a more autonomous system of guiding an inexperienced operator through an ultrasound study is needed. One example would be missions beyond low Earth orbit in which the time delay inherent with communication will make remote guidance impractical.

The Virtual Ultrasound Guidance system is a combination of hardware and

software. The hardware portion includes, but is not limited to, video glasses that allow hands-free, full-screen viewing. The glasses also allow the operator a substantial field of view below the glasses to view and operate the ultrasound system. The software is a comprehensive video program designed to guide an inexperienced operator through a detailed ultrasound or

echocardiographic study without extensive training or guidance from the ground. The program contains a detailed description using video and audio to demonstrate equipment controls, ergonomics of scanning, study protocol, and scanning guidance, including recovery from sub-optimal images.

The components used in the initial validation of the system include an Apple iPod Classic third-generation as the video source, and Myvue video glasses. Initially, the program prompts the operator to power-up the ultrasound

and position the patient. The operator would put on the video glasses and attach them to the video source. After turning on both devices and the ultrasound system, the audio-video guidance would then instruct on patient positioning and scanning techniques.

A detailed scanning protocol follows with descriptions and reference video of each view along with advice on technique. The program also instructs the operator regarding the types of images to store and how to overcome pitfalls in scanning. Images can be forwarded to

the ground or other site when convenient. Following study completion, the video glasses, video source, and ultrasound system are powered down and stored. Virtually any equipment that can play back video can be used to play back the program. This includes a DVD player, personal computer, and some MP3 players.

This work was done by Timothy Caine and David Martin of Johnson Space Center. Further information is contained in a TSP (see page 1). MSC-24800-1

Beat-to-Beat Blood Pressure Monitor

This invention is applicable to all segments of the blood pressure monitoring market, including ambulatory, home-based, and high-acuity monitoring.

Lyndon B. Johnson Space Center, Houston, TX

This device provides non-invasive beat-to-beat blood pressure measurements and can be worn over the upper arm for prolonged durations. Phase and waveform analyses are performed on filtered proximal and distal photoplethysmographic (PPG) waveforms obtained from the brachial artery. The phase analysis is used primarily for the computation of the mean arterial pressure, while the waveform analysis is used primarily to obtain the pulse pressure. Real-time compliance estimate is used to refine both the mean arterial and pulse pressures to provide the beat-to-beat blood pressure measurement.

This wearable physiological monitor can be used to continuously observe the beat-to-beat blood pressure (B3P). It can be used to monitor the effect of prolonged exposures to reduced gravitational environments and the effectiveness of various countermeasures.

A number of researchers have used pulse wave velocity (PWV) of blood in the arteries to infer the beat-to-beat blood pressure. There has been documentation of relative success, but a device that is able to provide the required accuracy and repeatability has not yet been developed. It has been demonstrated that an accurate and repeatable blood pressure measurement can be obtained by measuring the phase change (e.g., phase velocity), amplitude change, and distortion of the PPG waveforms along the brachial artery. The approach is based on comparing the full PPG waveform between two points along the

artery rather than measuring the time-of-flight. Minimizing the measurement separation and confining the measurement area to a single, well-defined artery allows the waveform to retain the general shape between the two measurement points. This allows signal processing of waveforms to determine the phase and amplitude changes.

Photoplethysmography, which measures changes in arterial blood volume, is commonly used to obtain heart rate and blood oxygen saturation. The digitized PPG signals are used as inputs into the beat-to-beat blood pressure measurement algorithm. The algorithm consists of the following main components:

- First harmonic isolation bandpass filters take the raw PPG signals and separate out the first harmonics.
- Three harmonic lowpass filters take the PPG signal and filter out all spectral components outside the first three harmonics. The first three harmonics are used for regeneration of the pulse pressure waveforms.
- Phase analysis engine takes the first harmonics of the PPG signals and computes the phase difference between them in real time using a cross-correlation-based algorithm. The phase difference is to the first order correlated to the MAP (mean arterial pressure).
- Compliance estimation engine takes information on the general shape of the waveforms and the phase delay to compute the local compliance of the artery. The higher the arterial pres-

sure, the higher the Young's modulus and thus the lower the compliance.

- MAP computation engine obtains the phase delay and compliance information and provides the mean arterial pressure.
- Waveform analysis engine takes the PPG signal containing the first three harmonics and provides the signal processing needed for compliance (elasticity) estimation and pulse pressure computation.
- Pulse pressure computation engine takes the filtered PPG signal and an estimate of the arterial compliance to regenerate the pulse waveform.
- B3P computation engine takes the MAP and the pulse pressure computations and combines them with a blood pressure model and calibration data to produce the final signal of interest — the beat-to-beat blood pressure.

This work was done by Yong Jin Lee of Linea Research Corporation for Johnson Space Center. Further information is contained in a TSP (see page 1).

In accordance with Public Law 96-517, the contractor has elected to retain title to this invention. Inquiries concerning rights for its commercial use should be addressed to:

*Linea Research Corporation
1020 Corporation Way
Suite 216
Palo Alto, CA 94303*

Refer to MSC-24601-1, volume and number of this Medical Design Briefs issue, and the page number.



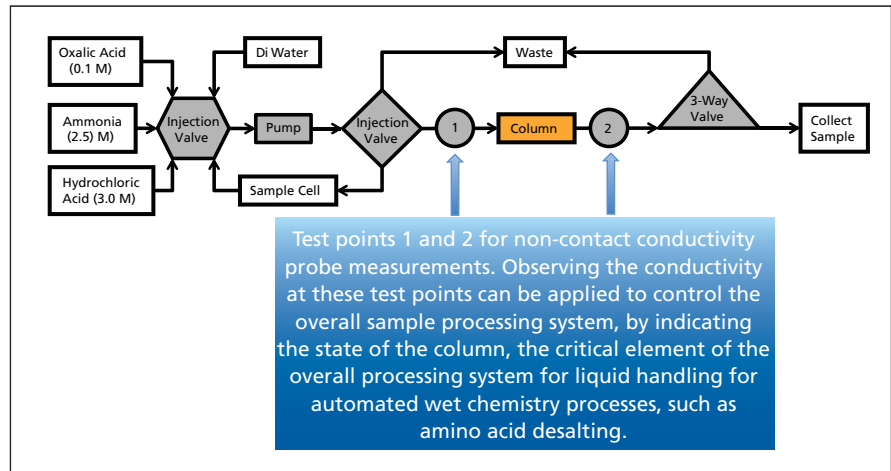
Non-Contact Conductivity Measurement for Automated Sample Processing Systems

Conductivity probes are used to control the process.

NASA's Jet Propulsion Laboratory, Pasadena, California

A new method has been developed for monitoring and control of automated sample processing and preparation especially focusing on desalting of samples before analytical analysis (described in more detail in "Automated Desalting Apparatus," (NPO-45428), NASA Tech Briefs, Vol. 34, No. 8 (August 2010), page 44). The use of non-contact conductivity probes, one at the inlet and one at the outlet of the solid phase sample preparation media, allows monitoring of the process, and acts as a trigger for the start of the next step in the sequence (see figure). At each step of the multi-step process, the system is flushed with low-conductivity water, which sets the system back to an overall low-conductivity state. This measurement then triggers the next stage of sample processing protocols, and greatly minimizes use of consumables.

In the case of amino acid sample preparation for desalting, the conductivity measurement will define three key conditions for the sample preparation process. First, when the system is neutralized (low conductivity, by washing with excess de-ionized water); second, when the system is acidified, by washing with a strong acid (high conductivity); and third, when the system is at a basic condition of high pH (high conductivity).



Test points 1 and 2 for non-contact conductivity probe measurements. Observing the conductivity at these test points can be applied to control the overall sample processing system, by indicating the state of the column, the critical element of the overall processing system for liquid handling for automated wet chemistry processes, such as amino acid desalting.

This System provides a new method of monitoring and control of automated sample processing and preparation.

When the system is acidified, by washing with a strong acid (high conductivity); and third, when the system is at a basic condition of high pH (high conductivity).

Taken together, this non-contact conductivity measurement for monitoring sample preparation will not only facilitate automation of the sample prepara-

tion and processing, but will also act as a way to optimize the operational time and use of consumables.

This work was done by Luther W. Beegle and James P. Kirby of Caltech for NASA's Jet Propulsion Laboratory. For more information, contact iaoffice@jpl.nasa.gov. NPO-47411

An MSK Radar Waveform

An increase in radar resolution results without the need for additional spectrum.

NASA's Jet Propulsion Laboratory, Pasadena, California

The minimum-shift-keying (MSK) radar waveform is formed by periodically extending a waveform that separately modulates the in-phase and quadrature-phase components of the carrier with offset pulse-shaped pseudo noise (PN) sequences. To generate this waveform, a pair of periodic PN sequences is each passed through a pulse-shaping filter with a half sinusoid impulse response. These shaped PN waveforms are then offset by half a chip time and are separately modulated on the in-phase

and quadrature phase components of an RF carrier. This new radar waveform allows an increase in radar resolution without the need for additional spectrum. In addition, it provides self-interference suppression and configurable peak sidelobes.

Compared strictly on the basis of the expressions for delay resolution, mainlobe bandwidth, effective Doppler bandwidth, and peak ambiguity sidelobe, it appears that bi-phase coded (BPC) outperforms the new MSK wave-

form. However, a radar waveform must meet certain constraints imposed by the transmission and reception of the modulation, as well as criteria dictated by the observation. In particular, the phase discontinuity of the BPC waveform presents a significant impediment to the achievement of finer resolutions in radar measurements — a limitation that is overcome by using the continuous phase MSK waveform. The phase continuity, and the lower fractional out-of-band power of MSK, increases the al-

lowable bandwidth compared with BPC, resulting in a factor of two increase in the range resolution of the radar. The MSK waveform also has been demonstrated to have an ambiguity sidelobe structure very similar to BPC, where the sidelobe levels can be decreased by increasing the length of the m-sequence used in its generation.

This ability to set the peak sidelobe level is advantageous as it allows the sys-

tem to be configured to a variety of targets, including those with a larger dynamic range. Other conventionally used waveforms that possess an even greater spectral efficiency than the MSK waveform, such as linear frequency modulation (LFM) and Costas frequency hopping, have a fixed peak sidelobe level that is therefore not configurable, and can be exceeded by high contrast targets. Furthermore, in the case of a mul-

tistatic experiment observing a target in motion, self-interference from the transmitter to the receiver is mitigated by the MSK waveform. Waveforms that have delay Doppler coupling, such as LFM, provide no such protection.

This work was done by Kevin J. Quirk and Meera Srinivasan of Caltech for NASA's Jet Propulsion Laboratory. For more information, contact iaoffice@jpl.nasa.gov. NPO-48367

Telescope Alignment From Sparsely Sampled Wavefront Measurements Over Pupil Subapertures

NASA's Jet Propulsion Laboratory, Pasadena, California

Alignment of two-element telescopes is a classic problem. During recent integration and test of the Space Interferometry Mission's (SIM's) Astrometric Beam Combiner (ABC), the innovators were faced with aligning two such telescope subsystems in the presence of a further complication: only two small subapertures in each telescope's pupil were accessible for measuring the wavefront with a Fizeau interferometer.

This meant that the familiar aberrations that might be interpreted to infer system misalignments could be viewed only over small sub-regions of the pupil, making them hard to recognize. Further, there was no contiguous surface of the pupil connecting these two subapertures, so relative phase piston information was lost; the underlying full-aperture aberrations therefore had an additional degree of ambiguity.

The solution presented here is to recognize that, in the absence of phase piston, the Zygo measurements primarily provide phase tilt in the subaperture windows of interest. Because these windows are small and situated far from the center of the (inaccessible) unobscured full aperture, any aberrations that are higher-order than tilt will be extremely high-order on the full aperture, and so not necessary or helpful to the alignment. Knowledge of the telescope's optical prescription allows straightforward evaluation of sensitivities (subap mode strength per unit full-aperture aberration), and these can be used in a predictive matrix approach to move with assurance to an aligned state.

The technique is novel in every operational way compared to the standard approach of alignment based on full-aper-

ture aberrations or searching for best rms wavefront. This approach is closely grounded in the observable quantities most appropriate to the problem. It is also more intuitive than inverting full phase maps (or subaperture Zernike spectra) with a ray-tracing program, which must certainly work in principle, but in practice met with limited success. Even if such classical alignment techniques became practical, the techniques reported here form a reassuringly transparent and intuitive check on the course of the alignment with very little computational effort.

This work was done by Eric. E. Bloemhof, Xin An, Gary M. Kuan, Douglas M. Moore, Joseph F. O'Shay, Hong Tang, and Norman A. Page of Caltech for NASA's Jet Propulsion Laboratory. For more information, contact iaoffice@jpl.nasa.gov. NPO-47814

Method to Remove Particulate Matter From Dusty Gases at Low Pressures

This method could be of use to the semiconductor industry to remove particles during low-pressure plasma processing.

John F. Kennedy Space Center, Florida

Future human exploration of Mars will rely on local Martian resources to reduce the mass, cost, and risk of space exploration launched from Earth. NASA's In Situ Resource Utilization (ISRU) Project seeks to produce mission consumables from local Martian resources, such as atmospheric gas. The Martian atmosphere, however, contains dust particles in the 2-to-10-micrometer range.

These dust particles must be removed before the Martian atmospheric gas can be processed. The low pressure of the Martian atmosphere, at 5 to 10 mbars, prevents the development of large voltages required for a standard electrostatic precipitator. If the voltage is increased too much, the corona transitions into a glow/streamer discharge unsuitable for the operation of a

precipitator. If the voltage is not large enough, the dust particles are not sufficiently charged and the field is not strong enough to drive the particles to the collector.

A method using electrostatic fields has been developed to collect dust from gaseous environments at low pressures, specifically carbon dioxide at pressures around 5 to 10 mbars. This method,

commonly known as electrostatic precipitation, is a mature technology in air at one atmosphere. In this case, the high voltages required for the method to work can easily be achieved. However, in carbon dioxide at low pressures, such as those found on Mars, large voltages are not possible.

The innovation reported here consists of two concentric cylindrical electrodes set at specific potential difference that generate an electric field that produces a corona capable of imparting an electrostatic charge to the incoming dust particles. The strength of the field is carefully balanced so as to produce a stable charging corona at 5 to 10 mbars, and is also capable of imparting a force to the particles that drives them to the collecting electrode.

There are only two possible ways that dust can be removed from Martian atmospheric gas intakes: with this electrostatic precipitator design, and with

the use of filters. However, filters require upstream compression of the gas to be treated because the atmospheric pressure on Mars is too close to vacuum to use a vacuum pump downstream to the filter to draw the gas through the filter. The electrostatic precipitator is the best and more efficient solution for this environment. No other precipitator designs have been developed for the environment of Mars due to the challenges of the low atmospheric pressure.

Dust particles are charged using corona generation around the high-voltage discharge electrode, which ionizes gas molecules. Since the atmospheric gas intakes for the ISRU processing chambers will likely be cylindrical, cylindrical precipitator geometry was chosen. The electrostatic precipitator design presented here removes simulated Martian dust particles in the required

range in a simulated Martian atmospheric environment. The current-voltage (I-V) characteristic curves taken for the nine precipitator configurations at 9 mbars of pressure showed that a cylindrical collecting electrode 7.0 cm in diameter with a concentric positive high-voltage electrode 100 μm thick provides the best range of voltage and charging corona current. This precipitator design is effective for the size of the dust particles expected in the Martian atmosphere. Mass determination, as well as microscopic images and particle size distributions of dust collected on a silicon wafer placed directly below the precipitator with the field on and off, showed excellent initial results.

This work was done by Carlos Calle of Kennedy Space Center, and Sid Clements of the Appalachian State University Department of Physics and Astronomy. Further information is contained in a TSP (see page 1), KSC-13657

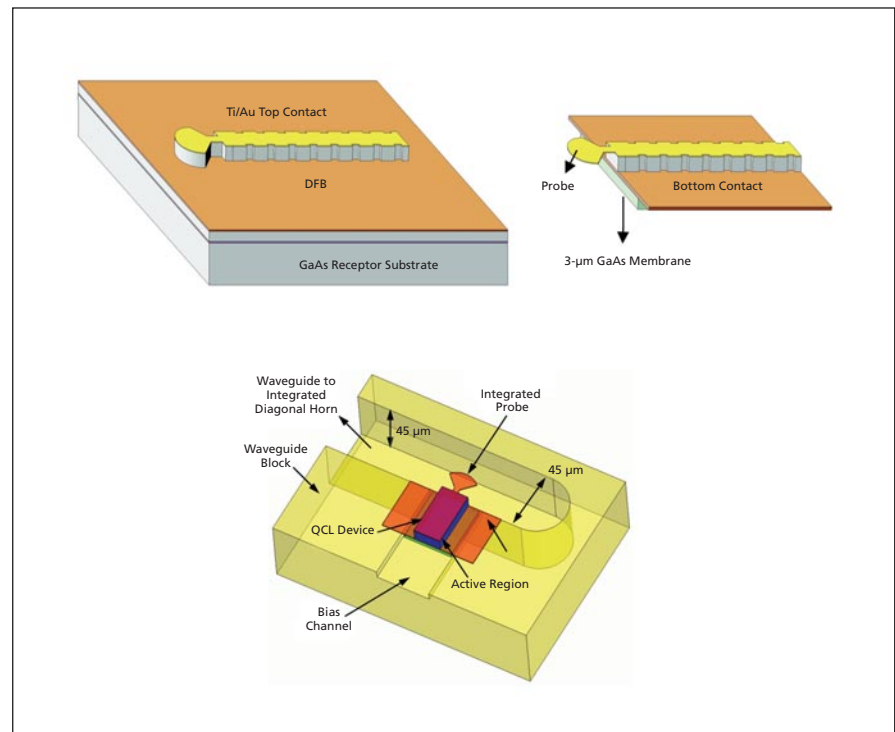
Terahertz Quantum Cascade Laser With Efficient Coupling and Beam Profile

High-power QCLs can be used in medical instruments, security screening equipment, and illicit material detection.

NASA's Jet Propulsion Laboratory, Pasadena, California

Quantum cascade lasers (QCLs) are unipolar semiconductor lasers, where the wavelength of emitted radiation is determined by the engineering of quantum states within the conduction band in coupled multiple-quantum-well heterostructures to have the desired energy separation. The recent development of terahertz QCLs has provided a new generation of solid-state sources for radiation in the terahertz frequency range. Terahertz QCLs have been demonstrated from 0.84 to 5.0 THz both in pulsed mode and continuous wave mode (CW mode).

A 2.7-THz QCL structure uses a metal-metal waveguide QCL with multiple-quantum-well cascade medium to provide terahertz gain for subbands engineered to have the desired energy separation. The approach employs a resonant-phonon depopulation concept. The metal-metal (MM) waveguide fabrication is performed using Cu-Cu thermo-compression bonding to bond the GaAs/AlGaAs epitaxial layer to a GaAs receptor wafer. A laterally corrugated distributed feedback (DFB) grating is etched into a MM waveguide, as



MM-Waveguide QCL Laser shown in (top) a processing schematic for fabrication of the laser with integrated waveguide probe; and (bottom) in a waveguide mount with the integrated radial probe. The top half of the block is removed to show the QCL device inside the waveguide.

this is easily performed in a single photolithographic and etch step. Extended modeling is done for both the DFB cavity and the coupling with the waveguide via the integrated probe. The DFB structure QCL has an integrated waveguide probe suitable for mounting in a machined waveguide block. Following fabrication of the MM-waveguide, the wafer can be mounted top-down on a temporary support wafer, and the GaAs receptor substrate is thinned to a membrane with the assistance of an etch-stop layer.

Development of a demonstrator horn-antenna coupled QCL at 2.7 THz with Gaussian output beam profile and high coupling efficiency capable of effectively pumping mixers at these frequencies is a

major breakthrough in the spectroscopic studies for the Earth-observation and astrophysics community. The approach, which includes an integrated probe on the QCL device in a waveguide enclosure transitioning to a diagonal horn, may lead to compact, coherent, continuous-wave solid-state sources.

A phase-locked terahertz QCL source with high-quality beam profile and excellent output coupling efficiency operating at or above liquid nitrogen temperatures will be of great strategic importance for NASA's astrophysics, Earth, and planetary mission capabilities. This will make these QCLs the local oscillator source of choice for the future NASA and European suborbital and or-

bitual terahertz instruments for astrophysics missions such as the interferometric (ESPRIT) and other single- and multi-pixel heterodyne spectroscopic missions, as well as for Earth observing and planetary missions. A high-power QCL with good beam profile can also be used in biological and medical science instruments, security screening and illicit material detection, and nondestructive evaluation applications.

This work was done by Goutam Chattopadhyay, Jonathan H. Kawamura, and Robert H. Lin of Caltech, and Benjamin Williams of UCLA for NASA's Jet Propulsion Laboratory. For more information, contact iaoffice@jpl.nasa.gov. NPO-46980

Measurement Via Optical Near-Nulling and Subaperture Stitching

This simple and universal technique uses adjustable corrective optics.

Goddard Space Flight Center, Greenbelt, Maryland

A subaperture stitching interferometer system provides near-nulling of a subaperture wavefront reflected from an object of interest over a portion of a surface of the object. A variable optical element located in the radiation path adjustably provides near-nulling to facilitate stitching of subaperture interferograms, creating an interferogram representative of the entire surface of interest. This enables testing of aspheric surfaces without null optics customized for each surface prescription.

The surface shapes of objects such as lenses and other precision components are often measured with interferometry. However, interferometers have a limited capture range, and thus the test wavefront cannot be too different from the reference or the interference cannot be analyzed. Furthermore, the performance of the interferometer is usually best when the test and reference wavefronts are nearly identical (referred to as a "null" condition). Thus, it is necessary when performing such measurements to correct for known variations in shape to ensure that unintended variations are within the capture range of the interferometer and accurately measured.

This invention is a system for near-nulling within a subaperture stitching interferometer, although in principle, the concept can be employed by wavefront-measuring gauges other than interferom-

eters. The system employs a light source for providing coherent radiation of a subaperture extent. An object of interest is placed to modify the radiation (e.g., to reflect or pass the radiation), and a variable optical element is located to interact with, and nearly null, the affected radiation. A detector or imaging device is situated to obtain interference patterns in the modified radiation. Multiple subaperture interferograms are taken and are "stitched," or joined, to provide an interferogram representative of the entire surface of the object of interest.

The primary aspect of the invention is the use of adjustable corrective optics in the context of subaperture stitching near-nulling interferometry, wherein a complex surface is analyzed via multiple, separate, overlapping interferograms. For complex surfaces, the problem of managing the identification and placement of corrective optics becomes even more pronounced, to the extent that in most cases the null corrector optics are specific to the particular asphere prescription and no others (i.e. another asphere requires completely different null correction optics). In principle, the near-nulling technique does not require subaperture stitching at all.

Building a near-null system that is practically useful relies on two key features: simplicity and universality. If the system is too complex, it will be diffi-

cult to calibrate and model its manufacturing errors, rendering it useless as a precision metrology tool and/or prohibitively expensive. If the system is not applicable to a wide range of test parts, then it does not provide significant value over conventional null-correction technology. Subaperture stitching enables simpler and more universal near-null systems to be effective, because a fraction of a surface is necessarily less complex than the whole surface (excepting the extreme case of a fractal surface description). The technique of near-nulling can significantly enhance aspheric subaperture stitching capability by allowing the interferometer to capture a wider range of aspheres. Moreover, subaperture stitching is essential to a truly effective near-nulling system, since looking at a fraction of the surface keeps the wavefront complexity within the capability of a relatively simple near-null apparatus. Furthermore, by reducing the subaperture size, the complexity of the measured wavefront can be reduced until it is within the capability of the near-null design.

This work was done by Greg Forbes, Gary De Vries, and Paul Murphy of QED Technologies, Inc.; and Chris Brophy of Optical Engineering Services for Goddard Space Flight Center. Further information is contained in a TSP (see page 1). GSC-16152-1

885-nm Pumped Ceramic Nd:YAG Master Oscillator Power Amplifier Laser System

Reduced thermal load results in a higher-performance laser.

Goddard Space Flight Center, Greenbelt, Maryland

The performance of a traditional diode pumped solid-state laser that is typically pumped with 808-nm laser diode array (LDA) and crystalline Nd:YAG was improved by using 885-nm LDAs and ceramic Nd:YAG. The advantage is lower quantum defect, which will improve the thermal loading on laser gain medium, resulting in a higher-performance laser. The use of ceramic Nd:YAG allows a higher Nd dopant level that will make up the lower absorption at the 885-nm wavelength on Nd:YAG.

When compared to traditional 808-nm pump, 885-nm diodes will have 30% less thermal load (or wasted heat) and will thus see a similar percentage improvement in the overall laser efficiency. In order to provide a more efficient laser system for future

flight missions that require the use of low-repetition-rate (<few hundred Hz) and high-energy laser pulses, laser diodes such as the 885-nm LDA were used for pumping the Nd:YAG laser crystal. This pumping scheme has many potential advantages for improved reliability, efficiency, thermal management, contamination control, and mechanical flexibility.

The advantages of using 885-nm pump diodes in Nd:YAG laser systems are numerous. The epitaxial structures of these 885-nm diodes are aluminum-free. There is a significant reduction in the thermal load generated from the Stokes shift or quantum defects. A Stokes shift is the energetic difference between the pump and laser photons. Pumping at a wavelength band closer to the lasing wavelength can

reduce the thermal load by $\approx 30\%$ compared to traditional pumping at 808 nm, and increase the optical-to-optical efficiency by the same factor. The slope efficiency is expected to increase with a reduction in the thermal load.

The typical crystalline Nd:YAG can be difficult to produce with doping level $>1\%$ Nd. To make certain that the absorption at 885 nm is on the same par as the 808-nm diode, the Nd:YAG material needs to be doped with higher concentration of Nd. Ceramic Nd:YAG is the only material that can be tailored to specific needs.

This work was done by Anthony Yu of Goddard Space Flight Center. Further information is contained in a TSP (see page 1). GSC-16205-1



Books & Reports

Airborne Hyperspectral Imaging System

A document discusses a hyperspectral imaging instrument package designed to be carried aboard a helicopter. It was developed to map the depths of Greenland's supraglacial lakes. The instrument is capable of telescoping to twice its original length, allowing it to be retracted with the door closed during take-off and landing, and manually extended in mid-flight. While extended, the instrument platform provides the attached hyperspectral imager a nadir-centered and unobstructed view of the ground.

Before flight, the instrument mount is retracted and securely strapped down to existing anchor points on the floor of the helicopter. When the helicopter reaches the destination lake, the door is opened and the instrument mount is manually extended. Power to the instrument package is turned on, and the data acquisition computer is commanded via a serial cable from an on-board user-operated laptop to begin data collection. After data collection is complete, the instrument package is powered down and the mount retracted, allowing the door to be closed in preparation for landing.

The present design for the instrument mount consists of a three-segment telescoping cantilever to allow for a sufficient extended length to see around the landing struts and provide a nadir-centered and unobstructed field of view for the hyperspectral imager. This instrument works on the premise that water preferentially absorbs light with longer wavelengths on the red side of the visible spectrum. This property can be exploited in order to remotely determine the depths of bodies of pure freshwater. An imager flying over such a lake receives light scattered from the surface, the bulk of the water column, and from the lake bottom. The strength of absorption of longer-wavelength light depends on the depth of the water column. Through calibration with *in situ* measurements of the water depths, a depth-determining algorithm may be

developed to determine lake depth from these spectral properties of the reflected sunlight.

This work was done by Alberto E. Behar and Moogega Cooper of Caltech; John Adler of NOAA; and Tobias Jacobson of the University of Southern California for NASA's Jet Propulsion Laboratory. Further information is contained in a TSP (see page 1). NPO-48141

Heat Shield Employing Cured Thermal Protection Material Blocks Bonded in a Large-Cell Honeycomb Matrix

A document describes a new way to integrate thermal protection materials on external surfaces of vehicles that experience the severe heating environments of atmospheric entry from space. Cured blocks of thermal protection materials are bonded into a compatible, large-cell honeycomb matrix that can be applied on the external surfaces of the vehicles. The honeycomb matrix cell size, and corresponding thermal protection material block size, is envisioned to be between 1 and 4 in. (≈ 2.5 and 10 cm) on a side, with a depth required to protect the vehicle. The cell wall thickness is thin, between 0.01 and 0.10 in. (≈ 0.025 and 0.25 cm).

A key feature is that the honeycomb matrix is attached to the vehicle's unprotected external surface prior to insertion of the thermal protection material blocks. The attachment integrity of the honeycomb can then be confirmed over the full range of temperature and loads that the vehicle will experience.

Another key feature of the innovation is the use of uniform-sized thermal protection material blocks. This feature allows for the mass production of these blocks at a size that is convenient for quality control inspection. The honeycomb that receives the blocks must have cells with a compatible set of internal dimensions. The innovation involves the use of a faceted subsurface under the honeycomb. This provides a predictable surface with perpendicular cell walls for the majority of the blocks. Some cells

will have positive tapers to accommodate mitered joints between honeycomb panels on each facet of the subsurface. These tapered cells have dimensions that may fall within the boundaries of the uniform-sized blocks.

This work was done by Peter Zell of Ames Research Center. Further information is contained in a TSP (see page 1). ARC-16018-1

Asymmetric Supercapacitor for Long-Duration Power Storage

A document discusses a project in which a series of novel hybrid positive electrode materials was developed and tested in asymmetric capacitors with carbon negative electrodes. The electrochemical performance of the hybrid capacitors was characterized by cyclic voltammetry and a DC charge/discharge test. The hybrid capacitor exhibited ideal capacitor behavior with an extended operating voltage of 1.6 V in aqueous electrolyte, and energy density higher than activated carbon-based supercapacitors.

Nanostructured MnO_2 is a promising material for electrochemical capacitors (ECS) because of its low cost, environmentally friendly nature, and reasonably high specific capacitance. The charge capacity of the capacitors can be further improved by increasing the specific surface area of the MnO_2 electrode material. The power density and space radiation stability of the capacitors can be enhanced by coating the MnO_2 nanoparticles with conducting polymers. The conducting polymer coating also helps in radiation-hardening the ECS.

This work was done by Krishnaswamy K. Rangan and Tirumalai S. Sudarshan of Materials Modification, Inc. for Glenn Research Center. Further information is contained in a TSP (see page 1).

Inquiries concerning rights for the commercial use of this invention should be addressed to NASA Glenn Research Center, Innovative Partnerships Office, Attn: Steven Fedor, Mail Stop 4-8, 21000 Brookpark Road, Cleveland, Ohio 44135. Refer to LEW-18751-1.



National Aeronautics and
Space Administration